Electronic Supplementary Information

GQD-Assisted MnO_6 Octahedra Engineering in $CuMnO_2$ for High Performance Coin-Cell Supercapacitor

Raushan Kabir[1,2], Sudipta Goswami[1], Dipten Bhattacharya[3], Saikat Kumar Seth[2], Chandan Kumar Ghosh[1,*]

[1]School of Materials Science and Nanotechnology, Jadavpur University, Jadavpur, Kolkata 700032, India

[2]Department of Physics, Jadavpur University, Jadavpur, Kolkata 700032, India

[3]Advanced Mechanical and Materials Characterization Division, CSIR-Central Glass and Ceramic Research Institute, Kolkata 700032, India

[*]Corresponding author's email ID: chandu_ju@yahoo.co.in

Table S1: Fit statistics and Structural details obtained from FullProf refinement of X-ray diffraction data and calculation

Sample name		**CCM0**	**CCM1**	**CCM2**
Lattice Parameters (Å)	a	a=5.5915	a=5.5454	a=5.5414
	b	b=2.89162	b=2.8847	b=2.8814
	c	c=5.91209	c=5.9019	c=5.9073
Bond Length (Å)	Mn-O	1.99 2.25	1.86 2.15	2.22 2.35
	Cu-O	1.78	2.00	1.43
Bond angle (Degree)	Mn-O-Mn	93.1 95.7	102.36 101.67	75.73 86.26
	Cu-O-Mn	122.7 121.3	116.49 115.27	146.87 118.98
	O-Mn-O	84.3 (4) 95.7 (4)	77.64 (4) 102.36 (4)	86.26 (4) 93.74 (4)

		93.1 (2) 86.9 (2) 180 (3)	101.66 (2) 78.33(2) 180 (3)	75.73 (2) 104.27 (2) 180 (3)
	O-Cu-O	180	180	180
Lattice volume (V) ($Å^3$)		92.751773	91.3656	91.2748
Average Crystallite Size (D)(nm)		23.46	20.34	15.58
Dislocation density (δ)		1.8E-3	2.4E-3	4.1E-3
Microstrain (Ɛ)		0.06	0.09	0.25
Reliability factors	x^2	3.4	3.5	3.1
	R_p	6.02	2.96	2.16
	R_{wp}	11.2	4.41	3.41

Table S2: Structural details obtained from TEM SAED pattern.

Sample name		**CCM0**	**CCM1**	**CCM2**
d_{hkl} (Å) corresponding to (11-1)		2.4298	2.4149	2.3895
d_{hkl} (Å) corresponding to (200)		2.6846	2.6511	2.6420
d_{hkl} (Å) corresponding to (11-3)		1.5564	1.5439	1.5295
Lattice Parameters (Å)	a	5.3692	5.3022	5.2840
	b	3.0971	3.0875	3.0459
	c	5.7327	5.6792	5.6309
Microstrain (Ɛ)		0.0369	0.0487	0.0522

Characterization of GQD sample:

The UV-Vis absorption spectra (Figure S1) of GQD displayed two peaks at 249 nm and 307 nm, which can be attributed to the π-π* transition of the aromatic sp^2 domain having bandgap values of 3.27 and 3.72 eV. The GQD Excitation-dependent photoluminescence (PL)

behaviour is a characteristic of fluorescent carbon materials. The GQD samples, when excited at 371 nm, displayed PL peaks at 469 and 525 nm, which are in good agreement with the literature. Figure S1(d) represents the Raman spectra of as-synthesised GQD samples, which feature two prominent peaks at 1441 and 1651 cm^{-1} corresponding to the D and G bands. These characteristics verify the successful synthesis of GQD [28-29, 35].

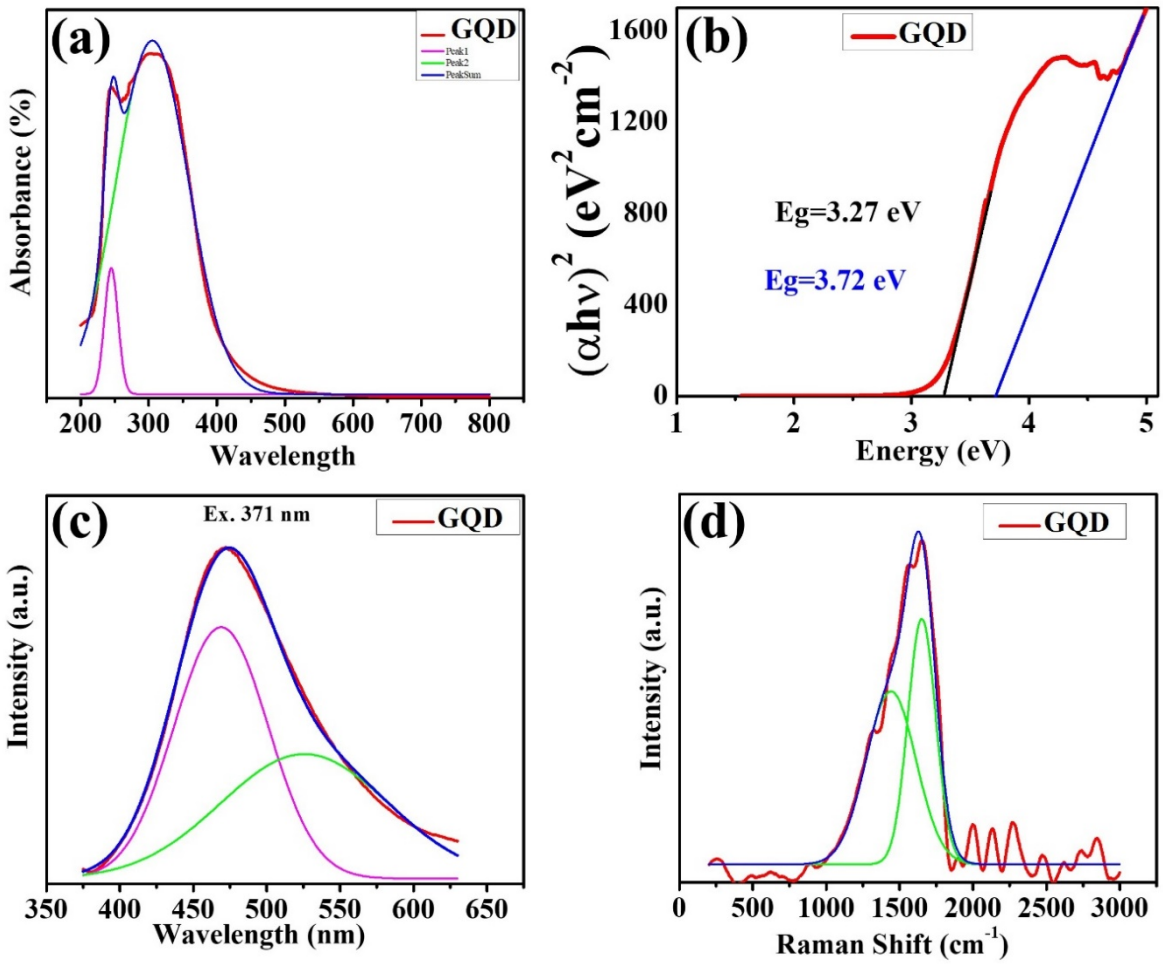

Figure S1: (a) UV-Vis. absorption spectra (b), corresponding band gaps (c) Photoluminescence spectra and (d) Raman spectra of the GQD sample.

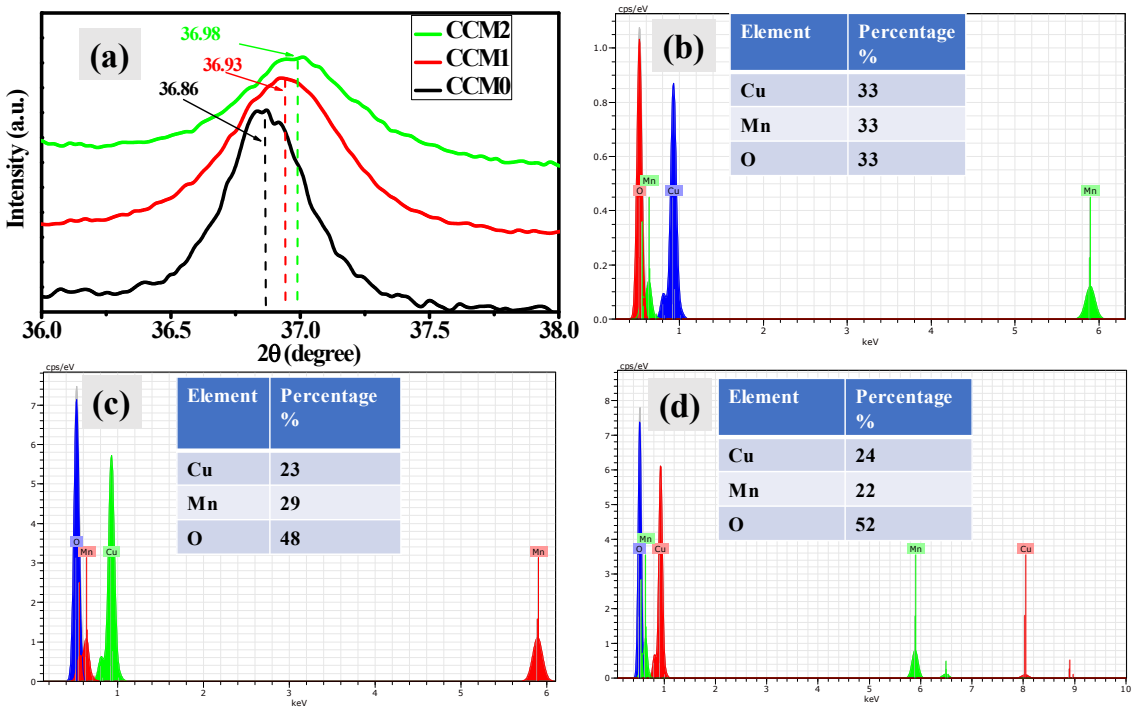

Figure S2: (a) XRD peak shifts and EDS plots of (b) CCM0, (c) CCM1, and (d) CCM2

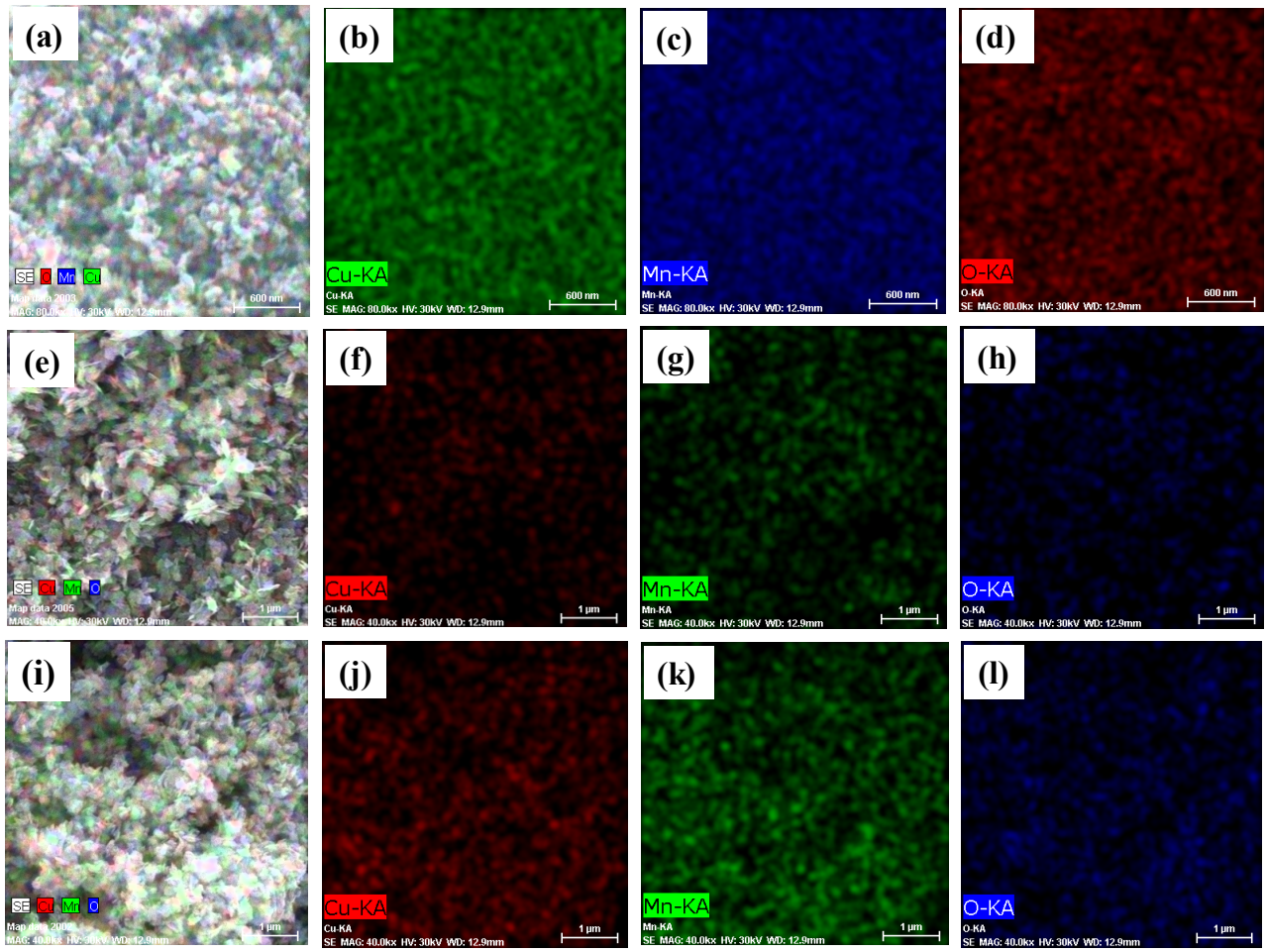

Figure S3: Elemental mapping of (a)-(d) CCM0, (e)-(h) CCM1 and (i)-(l) CCM2 samples.

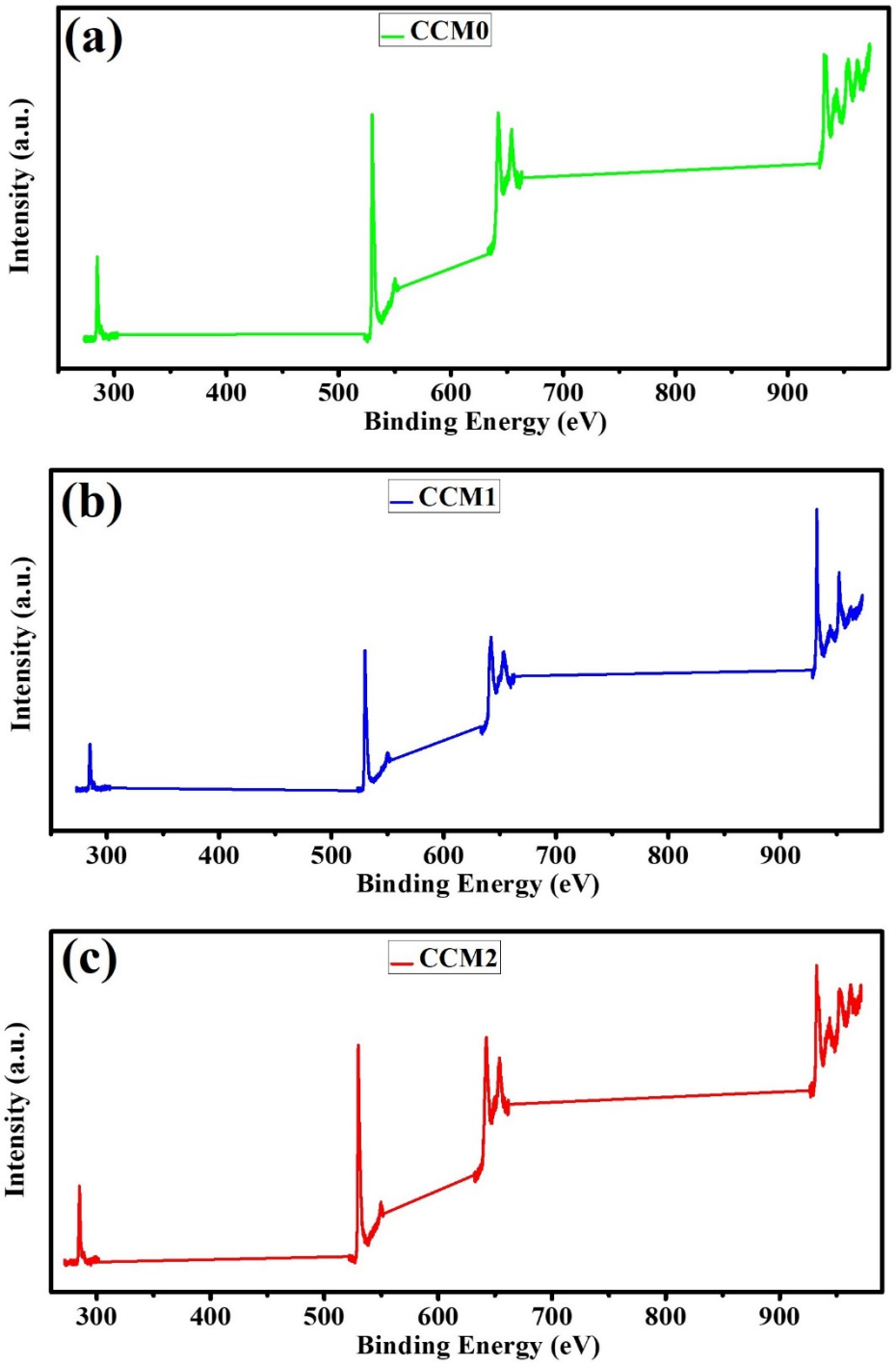

Figure S4: XPS Survey spectra

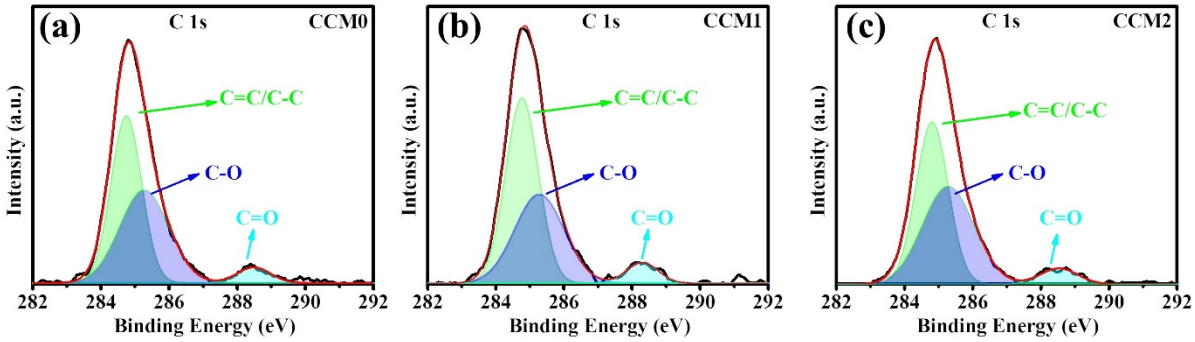

Figure S5: XPS spectra of C1s

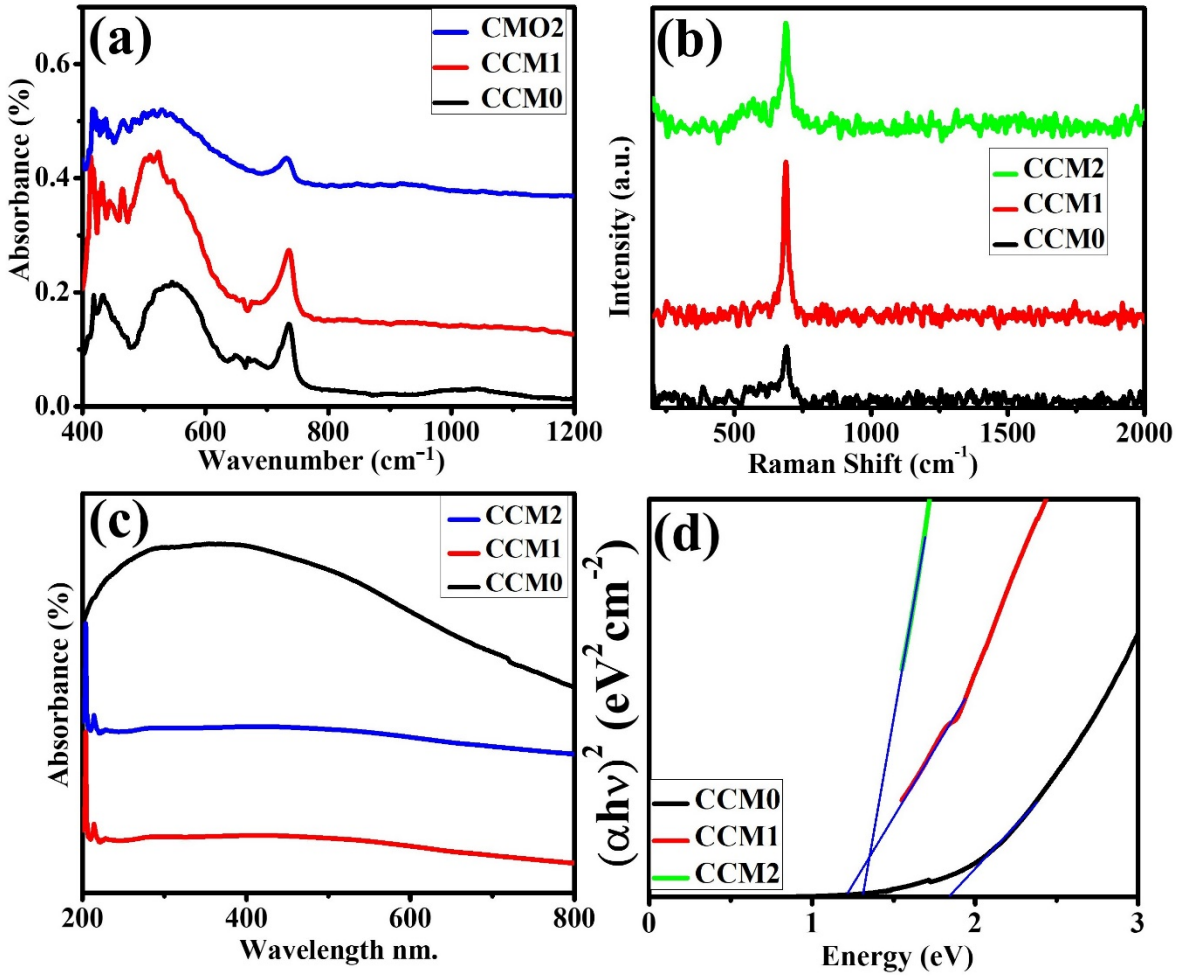

Figure S6: (a) FTIR spectra (400-1200 cm^{-1}), (b) Raman spectra from 250-2000 cm^{-1} (c) UV-Vis. absorption spectra (d) corresponding bandgap E_g

Electrochemical analysis

Coulombic efficiency (η%) is defined in this context as

$$\eta\% = \frac{t_{discharge}}{t_{charge}} \times 100 \quad \ldots \text{SE2}$$

where t_{charge} is the charging time and $t_{discharge}$ is the discharging time.

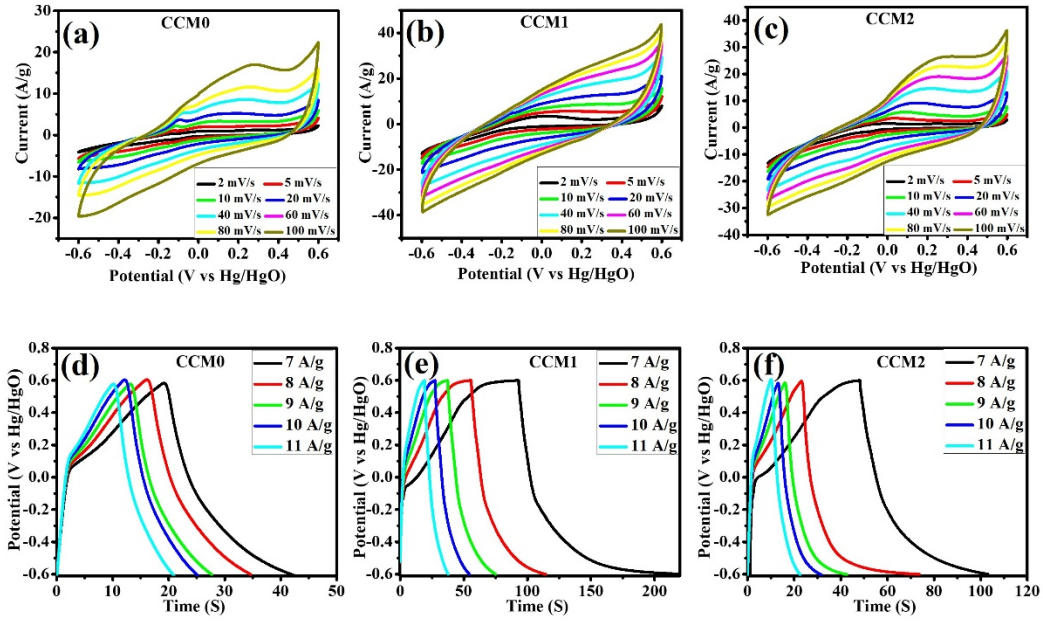

Figure S7: CV plots of (a) CCM0, (b) CCM1, and (c) CCM2 for different scan rates and GCD plots of (d) CCM0, (e) CCM1 and (f) CCM2 at different current densities.

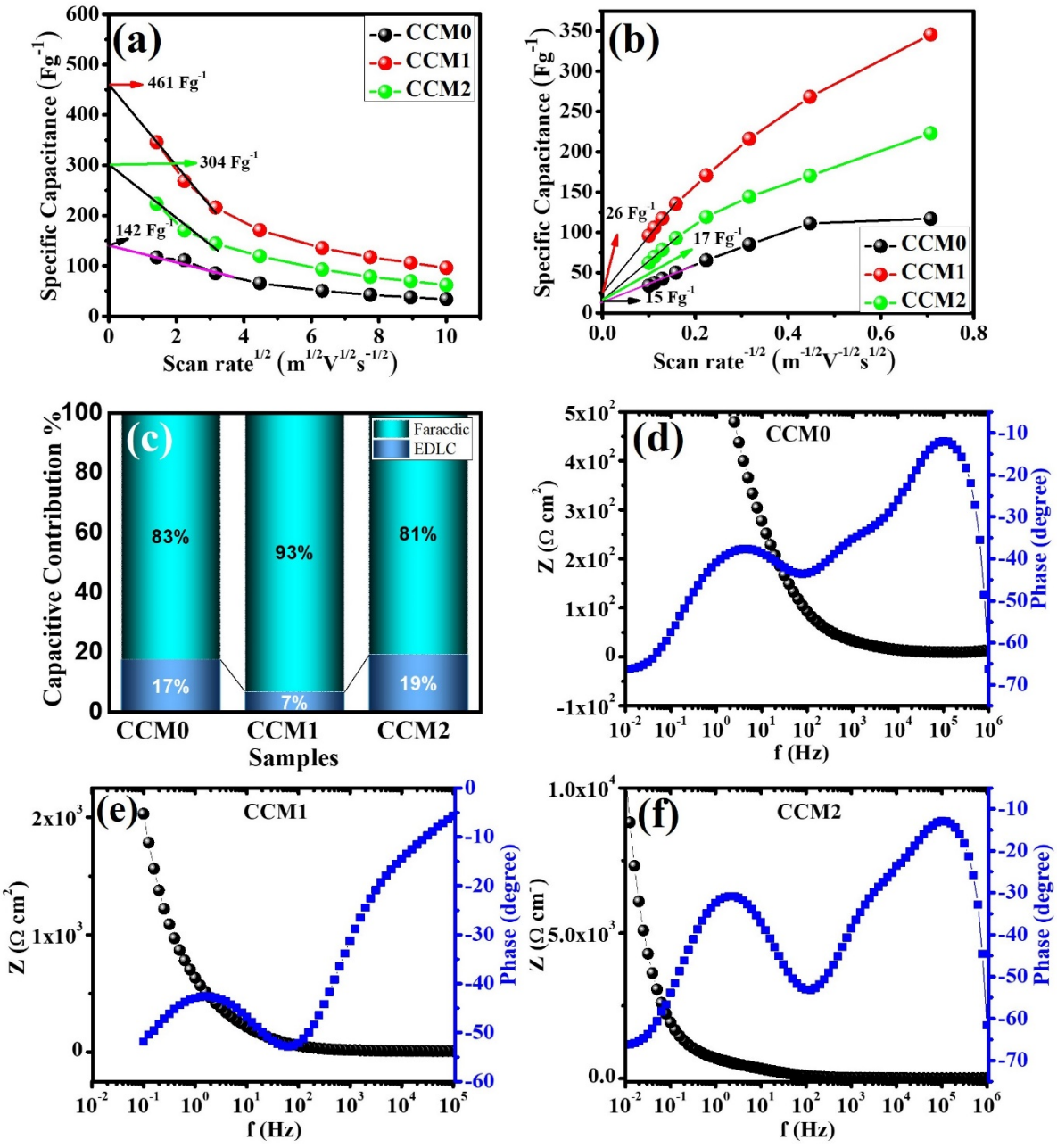

Figure S8: (a) C_m versus $\nu^{1/2}$ (b) C_m versus $\nu^{-1/2}$ plots (c) capacitance contribution percentage of CCM0, CCM1 and CCM2 and bode plot of (d) CCM0, (e) CCM1 and (f) CCM2

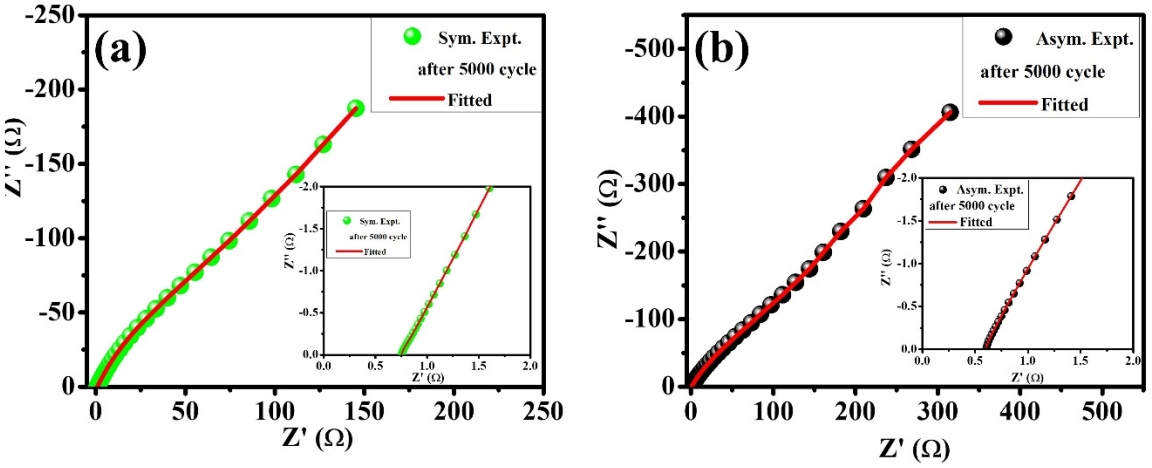

Figure S9: EIS plots after 5000 cycles of (a) symmetric and (b) asymmetric coin-cell supercapacitor

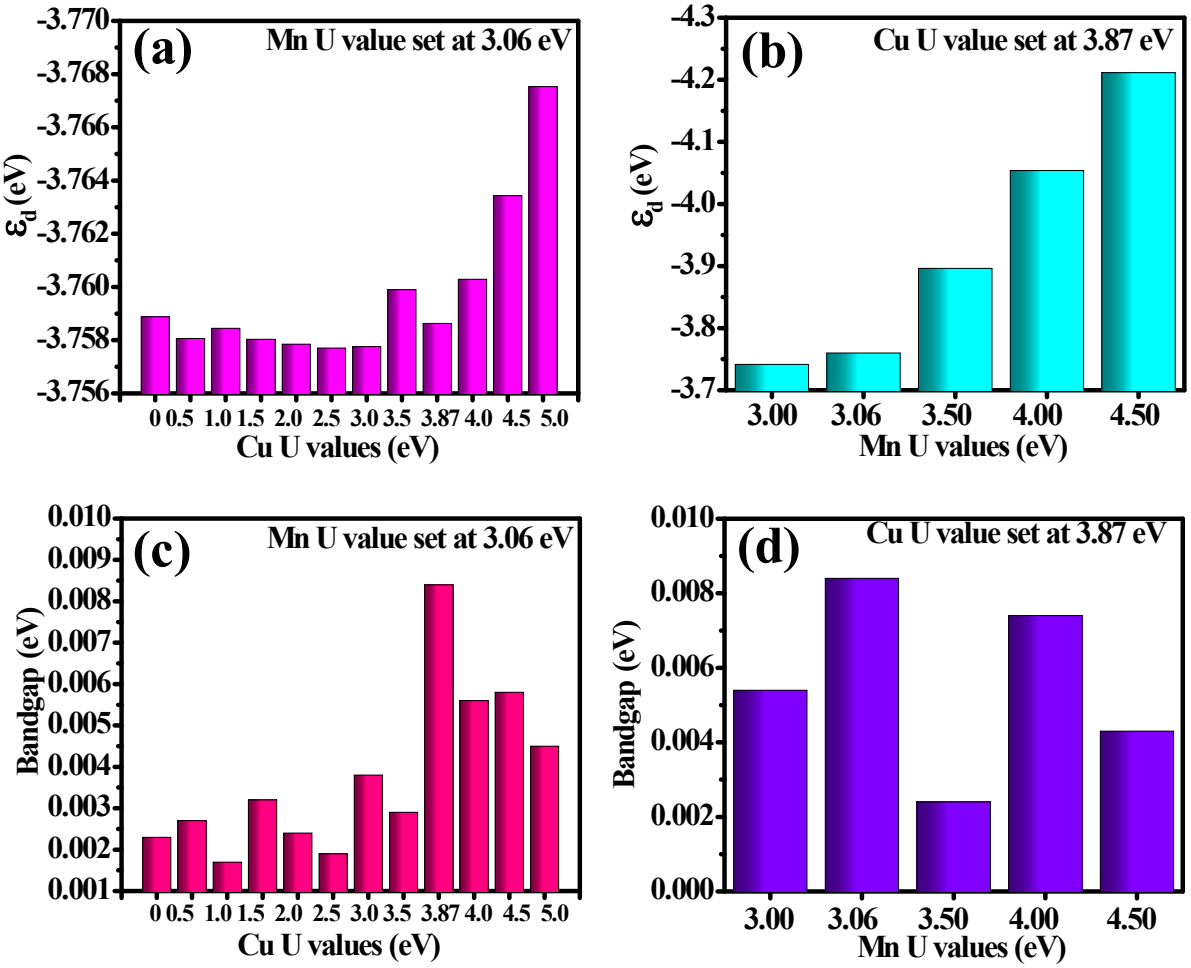

Figure S10: Variation of d-band centre position with (a) Cu U value and (b) Mn U value, and Variation of bandgap value with (a) Cu U value and (b) Mn U value.

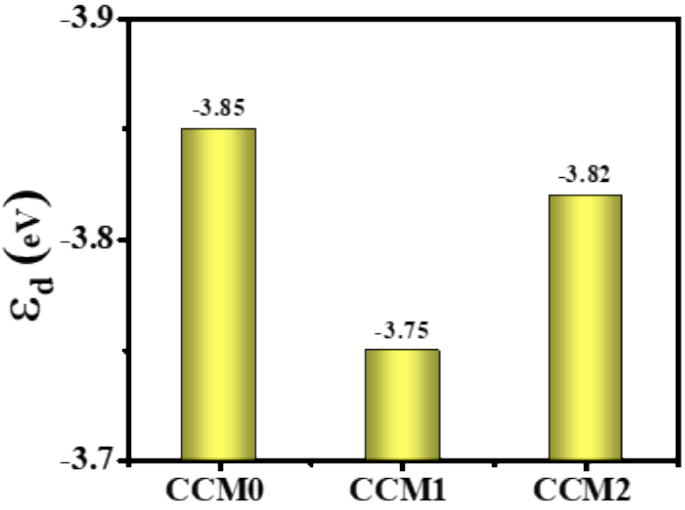

Figure S11: variation of d-band centre position

Table S3. Comparative analysis of the specific capacitance of the CCM1 electrode with other $CuMnO_2$-based electrodes, measured in 3 electrode configurations.

Electrode	**Electrode material deposited on**	**Electrolyte**	**Capacitance (F/g)**	**Reference**
$CuMnO_2$	Glassy carbon	1M Na_2SO_4	130.72 F/g at 0.2 A/g	S1
$CuMnO_2$	Nickel foam	PVA-KOH	765 F/g at 5 A/g	S2
CuMnO2-rGO	Nickel Foam	2M KOH	1727.15 F/g at 3A/g	S3
CuMnO2/GQD	Nickel Foam	3M KOH	520.2 at 1A/g	S4
PANI@CuMnO2 composite	Carbon cloth	0.1M H_2SO_4	355.62 mF/cm^2 at 1mA/cm^2	S5
CuMnO2-GQD	Glassy carbon	3M KOH	771 F/g	This work

Table S4. Comparative analysis of power and energy density of the CCM1 electrode with other Cu-based delafossites in 3 electrode configuration.

Electrode	Energy and Power density	Reference
$CuMnO_2$	14.71Wh/Kg at 90 W/kg	S1
$CuMnO_2$/PANI	130 W/kg at 773 W/kg	S6
$CuMnO_2$	15.5 Wh/Kg at 800 W Kg^{-1}	S7
$CuFeO_2$	30.55 Wh/kg and ~ 236.52 W/kg	S8
$CuFeO_2$	66.56 Wh/kg	S9
CuMnO2-GQD	154.35 Wh/Kg at 4200 W/Kg	This work

Table S5. Fit statistics and comparative analysis of equivalent circuit parameters of symmetric and asymmetric coin cell supercapacitor

System	Equivalent circuit	R_s (Ω)	R_{ct} (Ω)
Symmetric Fresh	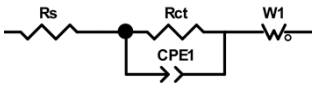	0.511	43.03
Symmetric after 5000 cycles		0.745	59.37
Asymmetric Fresh		0.435	32.32
Asymmetric after 5000 cycles		0.568	103.6

Table S6. Comparative analysis of CCM1-based symmetric and asymmetric coin-cell supercapacitor with other symmetric and asymmetric devices

Material	System	Electrolyte	Capacitance (F/g)	Current density (A/g)	Energy density (W hr/kg)	Power density (W/kg)	Reference

$CuMnO_2$	Symmetric Coin cell	Aqueous 1M Na_2SO_4	71	0.35	14.2	333.3	S1
Antimony trioxide (Sb2O3)	Symmetric Coin cell	Aqueous 6M KOH	354.4	1	9.21	300	S10
PICACIFF-activated carbon	Symmetric Coin cell	Ethylene glycol-based aqueous electrolyte	30	100 mA/g	9.4	230	S11
N doped carbon	Symmetric	Aqueous 6M KOH	359.9	1	18.9	500	S12
Titaniumoxynitride (TiON) nanorods	Symmetric Coin cell	1MLiClO4	1930 mF/g^{-1}	250 mAg^{-1}	6.7	180	S13
rGO/AuNPs	Symmetric Coin cell	Aqueous 6M KOH	56.09	-------	7.79	2512	S14
$BiMnO_3$//AC	Asymmetric	Aqueous 3M KOH	108 F/cm^2	0.25 $mAcm^{-2}$	14.4	50	S15
$ZnNi_2O_4/WS_2$//AC	Asymmetric	NaOH	171.3	--------	61	1236	S16
$CuMnO_2$/ GQD	Symmetric Coin cell	Aqueous 3M KOH	145	1	34.2	650	This work
$CuMnO_2$/ GQD//AC	Asymmetric Coin cell	Aqueous 3M KOH	147	2	40.01	1398	This work

Reference:

(S1) R. Kabir, R. Begum, K. R. Sahoo, S. Goswami, S. N. Das, M. R. Karim, D. Bhattacharya, S. Seth, C. K. Ghosh, Nanoarchitectonics of Interstitial Oxygen and Jahn–Teller Distortion to Enhance Electrochemical Performance of $CuMnO_2$: Symmetric Coin-Cell**,** *Appl. Phys. A*, 2025, **131**(1), 1–15, DOI: 10.1007/s00339-024-08116-z.

(S2) S. Fu, L. Li, Y. Jing, Y. Zhang, X. Wang, S. Fang, J. Wang, G. Li, Crystal Growth of Bimetallic Oxides $CuMnO_2$ With Tailored Valence States for Optimum Electrochemical Energy Storage**,** *Cryst. Growth Des.*, 2018, **18**(10), 6107–6116, DOI: 10.1021/acs.cgd.8b00988.

(S3) F. Bahmani, S. H. Kazemi, Y. Wu, L. Liu, Y. Xu, Y. Lei, $CuMnO_2$–Reduced Graphene Oxide Nanocomposite as A Free-Standing Electrode for High-Performance Supercapacitors**,** *Chem. Eng. J.*, 2019, **375**, 121966, DOI: 10.1016/j.cej.2019.121966.

(S4) M. Ashourdan, A. Semnani, F. Hasanpour, S. E. Moosavifard, Synthesis of $CuMnO_2$/Graphene Quantum Dot Nanocomposites as Novel Electrode Materials for High Performance Supercapacitors**,** *J. Energy Storage*, 2021, **36**, 102449, DOI: 10.1016/j.est.2021.102449.

(S5) M. S. Chaudhary, D. Seth, S. Waris, S. Hasan, S. Sultana, M. A. Haider, M. Agarwal, M. Z. Khan, Hydrothermally Synthesized PANI-Decorated $CuMnO_2$ Nanostructured Electrode: Powering Flexible Solid-State Supercapacitors for Wearable and Portable Electronics**,** *ACS Appl. Energy Mater.*, 2024, **8**(1), 245–258, DOI: 10.1021/acsaem.4c02311.

(S6) M. Arif, A. Bibi, I. Safra, A. Kumar, J. Makasana, S. Ballal, R. S. K. Sharma, P. K. Pathak and R. R. Chaudhary, Preparation of delafossite $CuMnO_2$ and polyaniline nanohybrid electrode for asymmetric supercapacitor, *J. Inorg. Organomet. Polym. Mater.*, 2025, **35**(8), 6643–6658. DOI: 10.1007/s10904-025-03684-w

(S7) K. S. Modi, P. B. Patel, D. Patel, J. Patel, V. Solanki and M. H. Patel, Electrochemical study of crednerite $CuMnO_2$ for symmetric supercapacitor applications, *Phys. Chem. Chem. Phys.*, 2026 DOI: 10.1039/D5CP04565G

(S8) A. Dey, S. Goswami, S. N. Das, D. Bhattacharya and C. K. Ghosh, Cu^{2+} at the surface/sub-surface region of $CuFeO_2$ rhombohedral nanostructures facilitates specific capacitance (~611 F g^{-1}): an understanding of the solvation energy dependent charge transfer mechanism, *Physica B: Condens. Matter*, 2023, **667**, 415207. DOI: 10.1016/j.physb.2023.415207

(S9) M. Danish, A. Hussain, S. R. Shafqat, Z. A. Sandhu, K. M. Batoo, M. F. Ijaz, A. H. Bhalli and M. Fiaz, Multifunctional $CuFeO_2$ nanocomposites: 3D series-metal-based materials for hydrogen evolution reaction and supercapacitor applications, *Ceram. Int.*, 2025, **51**(18), 24989–24998. DOI: 10.1016/j.ceramint.2025.03.180

(S10) U. Şahintürk, B. Üstün, H. Aydın, S. N. Koç, Ü. Kurtan, Coin Cell Constructed Symmetric Supercapacitor Based on Binder-Free Antimony Trioxide (Sb_2O_3) In Heteroatom Doped Carbon Nanofibers, *J. Power Sources*, 2024, **613**, 234882, DOI: 10.1016/j.jpowsour.2024.234882.

(S11) C. Ramasamy, J. P. Del Val, M. Anderson, An Analysis of Ethylene Glycol–Aqueous Based Electrolyte System for Supercapacitor Applications, *J. Power Sources*, 2014, **248**, 370–377, DOI: 10.1016/j.jpowsour.2013.09.078.

(S12) T. Ren, K. Wang, X. Lian, C. Xu, H. Niu, Nitrogen-Doped Carbon Nanotubes on Carbon Nanofibers for Applications as Supercapacitors with Long Lifetimes, *ACS Appl. Nano Mater.*, 2025, **8**, 11359–11369, DOI: 10.1021/acsanm.5c01120.

(S13) J. S. Samdani, T. H. Kang, B. J. Lee, Y. H. Jang, J. S. Yu, S. Shanmugam, Heterostructured Titanium Oxynitride–Manganese Cobalt Oxide Nanorods as High-Performance Electrode Materials for Supercapacitor Devices**,** *ACS Appl. Mater. Interfaces*, 2020, **12**, 54524–54536, DOI: 10.1021/acsami.0c13803.

(S14) L. Vivas, D. P. Singh, A Highly Efficient Graphene–Gold Based Green Supercapacitor Coin Cell Device for Energy Storage**,** *Front. Energy Res.*, 2022, **9**, 794604, DOI: 10.3389/fenrg.2021.794604.

(S15) A. M. Teli, T. S. Bhat, S. A. Beknalkar, S. M. Mane, L. S. Chaudhary, D. S. Patil, S. A. Pawar, H. Efstathiadis, J. C. Shin, Bismuth Manganese Oxide-Based Electrodes for Asymmetric Coin Cell Supercapacitor, *Chem. Eng. J.*, 2022, **430**, 133138, DOI: 10.1016/j.cej.2021.133138.

(S16) M. Sharma, M. Pershaanaa, A. K. Singh, R. Kasi, R. T. Subramaniam, P. Deb, $ZnNi_2O_4/WS_2$ Nanoflake-Based Electrodes for Quasi-Solid-State Asymmetric Supercapacitors, *ACS Appl. Nano Mater.*, 2024, **7**, 23592–23603, DOI: 10.1021/acsanm.4c03750.